Drug Design, Development and Therapy

Dovepress
open access to scientific and medical research

Open Access Full Text Article

ORIGINAL RESEARCH

Synergistic Anticancer Strategy of Sonodynamic Therapy Combined with PI-103 Against Hepatocellular Carcinoma

This article was published in the following Dove Press journal:
Drug Design, Development and Therapy

Huajing Yang
Hui Jing
Xue Han
Haoyan Tan
Wen Cheng

Department of Ultrasound, Harbin Medical University Cancer Hospital, Harbin, Heilongjiang Province, 150081, People's Republic of China

Purpose: Sonodynamic therapy (SDT) is considered a promising therapeutic strategy for the effective elimination of cancer cells. However, developing novel sonosensitizers with potentially high SDT efficacy remains a considerable challenge. Herein, we utilized near-infrared dye IR820 nanobubbles (NBs) combined with a dual PI3K/mTOR inhibitor PI-103 for the SDT treatment of hepatocellular carcinoma (HCC) in vitro.

Methods: The generated reactive oxygen species (ROS) were quantified using 2,7-dichlorodihydrofluorescein diacetate to determine the feasibility of using IR820 NBs as a potential sonosensitizer. The inhibition effects of the synergistic therapy was examined using the cell counting Kit 8 assay and apoptosis assay. JC-1 staining was performed to study mitochondrial membrane depolarization, and the transwell assay was used for cell migration analysis.

Results: The particle size and zeta potential of IR820 NBs were 545.5±93.1 nm and −5.19 ±1.73 mV, respectively. ROS accumulation was observed after HepG2 cells were treated with IR820 NBs under ultrasound irradiation. The SDT combined with PI-103 group inhibited cell viability and migration more strongly than the other groups ($P < 0.01$). The apoptosis assay also demonstrated a relatively high anti-HCC efficacy with the synergistic therapy, while JC-1 staining showed a decrease in the mitochondrial membrane potential after the combined treatment.

Conclusion: The combination of SDT and PI-103 was very effective in suppressing HCC proliferation, which might help develop new minimally invasive cancer treatment strategies.

Keywords: minimally invasive cancer treatment strategy, sonosensitizer, PI3K/mTOR inhibitor, IR820 nanobubbles

Introduction

Liver cancer is the sixth most common cancer and the fourth leading cause of cancer-related deaths worldwide. Hepatocellular carcinoma (HCC) is the predominant subtype of liver cancer, and approximately 85% of liver cancer patients suffer from it.[1] The main HCC treatment methods include surgical resection, radiation therapy, and chemotherapy; however, all these treatment modalities have limitations. As HCC is relatively insensitive to chemotherapy, it is usually treated by surgery. Meanwhile, only one third of all patients are good candidates for surgery due to the high invasiveness of the procedure and rapid HCC progression.[2] Therefore, there is an urgent need for the development of novel HCC therapeutic methods. Sonodynamic therapy (SDT) is a promising non-invasive approach using low-intensity ultrasound (US) and sonosensitizers to

Correspondence: Wen Cheng
Department of Ultrasound, Harbin Medical University Cancer Hospital, No. 150, Haping Road, Nangang District, Harbin, Heilongjiang Province, 150081, People's Republic of China
Tel +86 13313677182
Fax +86 451 85718392
Email hrbchengwen@163.com

submit your manuscript | www.dovepress.com
DovePress
http://doi.org/10.2147/DDDT.S296880

produce reactive oxygen species (ROS) that effectively induce the apoptosis of tumour cells.[3] In contrast to photodynamic therapy (PDT), SDT utilizes US to penetrate tumour tissues and carefully eliminate cancer cells while causing minimal damage to the adjacent normal tissues.[4,5]

According to the results of previous SDT studies, proper identification and development of novel sonosensitizers are among the most essential factors affecting the SDT efficacy.[6] The majority of known sonosensitizers were originally developed from photosensitizers used in PDT, such as hematoporphyrin, protoporphyrin, and near-infrared (NIR) dye. As a derivative of NIR dye indocyanine green (ICG), new indocyanine green (IR820) with enhanced stability and prolonged circulation time has attracted significant attention from researchers.[7,8] However, the shortcomings of IR820 (including poor solubility and lack of distribution specificity) considerably limit its practical application.[9] To mitigate these issues, various nanoparticles, such as nanobubbles (NBs), have been introduced as vehicles of therapeutic agents to increase their biocompatibility and the ultrasound targeted nanobubble destruction (UTND) method has become a promising therapeutic application in cancer treatment.[10,11] It was also found that sonosensitizer-conjugated NBs could effectively promote the SDT-induced ROS production for the precise targeting of tumour tissue.[12,13] Hence, in this study we have investigated the feasibility of using IR820 as a SDT sonosensitizer. To the best of our knowledge, this is the first report on the application of IR820 NB-mediated SDT for HCC treatment.

As SDT alone is not able to completely eradicate cancer cells due to the complex pathogenesis of HCC, combined therapy is usually adopted to increase antitumour activity and avoid possible adverse effects.[14] The PI3K/AKT/mTOR signalling pathway plays a pivotal role in the regulation of tumour cell proliferation and protein synthesis and is confirmed to be active in 30–50% of HCC cases.[15] As a dual PI3K/mTOR inhibitor, PI-103 was previously used in pre-clinical studies and exhibited a high inhibitory potential for HCC therapy.[16] In addition, accumulated ROS were utilized for the suppression of the PI3K/AKT/mTOR signalling pathway.[17] Therefore, we rationally designed a powerful antitumour strategy involving the comprehensive integration of SDT and PI-103 to develop a potential treatment for HCC with high therapeutic value.

The present study aimed to evaluate the synergistic therapeutic effects of the IR820 NB-mediated SDT and PI-103 for HCC treatment. The obtained results revealed that SDT combined with PI-103 not only promoted cell apoptosis through the loss of mitochondrial membrane potential, but also reduced cell viability and migration of HepG2 cells. Our findings suggest that the combination of SDT and suppression of the PI3K/AKT/mTOR signalling pathway may open new avenues in the development of non-invasive HCC treatment methods.

Materials and Methods

Fabrication and Characterization of IR820 NBs

IR820 NBs were prepared from 1,2-distearoyl-sn-glycero -3-phosphocholine (DSPC), 1,2-distearoyl-sn-glycero -3-phosphoethanolamine (DSPE), and IR820 combined at a molar ratio of 18:2:1. Appropriate amounts of these reagents were dissolved in chloroform and methyl alcohol, and the resulting mixture was subsequently evaporated at a temperature of 37 °C. The dried phospholipid blend was hydrated with 4 mL of phosphate-buffered saline (PBS) in a sealed vial at 55 °C, after which the air inside the vial was replaced with perfluoropropane (C_3F_8; Research Institute of Physical and Chemical Engineering of Nuclear Industry, Tianjin, China) using a syringe. Finally, the vial was mechanically vibrated in a dental amalgamator (YJT Medical Apparatuses and Instruments, Shanghai, China) for 60 s at a frequency of 60 Hz. The obtained IR820 NBs were collected by centrifugation at a speed of 500 rpm for 5 min and dispersed in fresh PBS for further analysis (Figure 1A).

After fabrication, the morphology of IR820 NBs was observed by transmission electron microscopy (TEM, Hitachi TEM system, Japan). Their hydrodynamic diameter, polydispersity index (PDI), and zeta potential were determined by dynamic light scattering (DLS) using a particle size analyzer (Anton Paar, Litesizer™ 500). Absorption spectra were recorded by a DU-640 ultraviolet–visible spectrophotometer (Beckman Coulter Inc., Brea, CA). To further evaluate the stability of IR820 NBs, they were stored at 37 °C for 48 h and then observed by TEM (Hitachi TEM system, Japan).

In vitro US Destructibility of IR820 NBs

UTND was evaluated using a previously reported method.[18] NBs were exposed to US with a frequency of 1 MHz and an output intensity of 3 W/cm^2 using a 20 mm

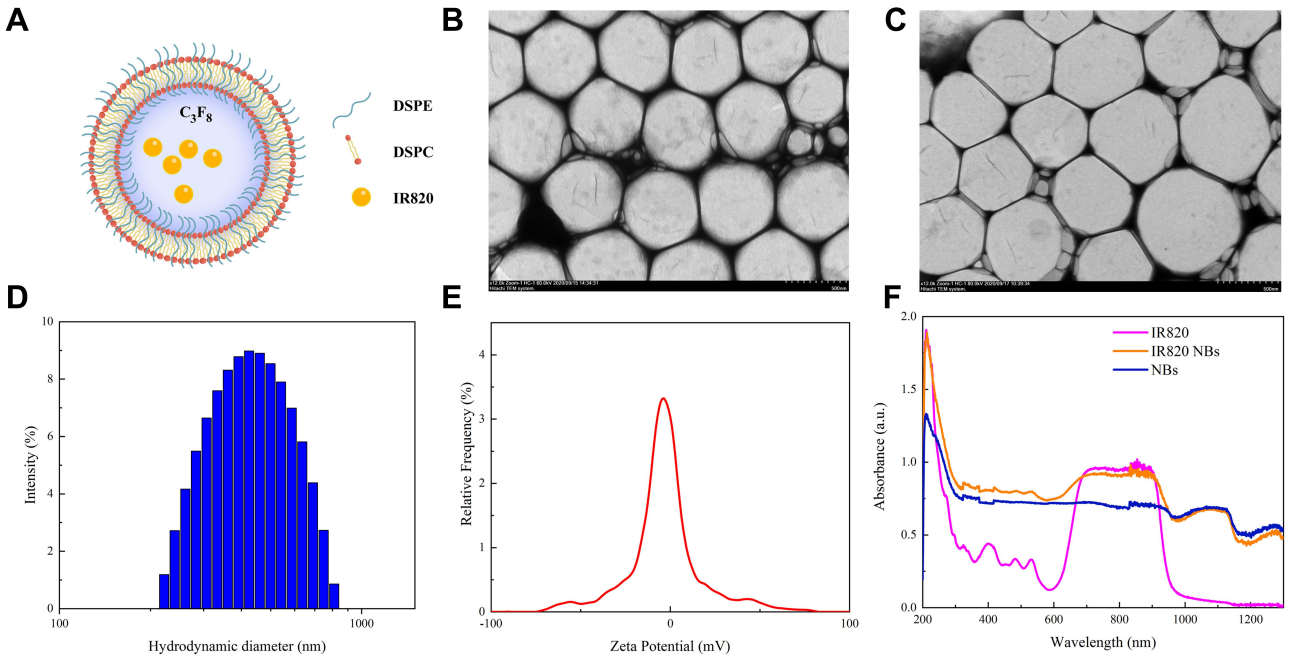

Figure 1 Fabrication and characterization of IR820 NBs. (**A**) The microstructural schematic diagram of IR820 NBs. (**B**) Transmission electron microscopy (TEM) image of IR820 NBs. (**C**) TEM image of IR820 NBs after stored at 37 °C for 48 h. (**D**) Hydrodynamic diameter of IR820 NBs measured by DLS. (**E**) Zeta potential of IR820 NBs. (**F**) Absorption spectra of IR820, IR820 NBs and NBs.

probe (Institute of Ultrasound Imaging, Second Affiliated Hospital of Chongqing Medical University, Chongqing, China). Each sonication cycle contained 4 frames of 30 s at a duty cycle of 50%. The concentration of NBs after US irradiation were determined by a hemocytometer.

Cell Culture

The human HCC cell line, HepG2, was obtained from the Institute of Cancer Research affiliated with the Harbin Medical University and approved by Ethics Committee of Harbin Medical University. The HepG2 cells were cultured in Dulbecco's Modified Eagle Medium (DMEM, Hyclone, Logan, UT, USA) supplemented with 10% fetal bovine serum (FBS, Gibco, Carlsbad, CA) in a humidified incubator containing 5% carbon dioxide at 37 °C.

Detection of Intracellular ROS Generation

Intracellular ROS generation was examined using 2,7-dichlorodihydrofluorescein diacetate (DCFH–DA, Applygen Technologies Inc., Beijing, PR China) as an indicator. After 6 h of treatment, HepG2 cells were loaded with DCFH–DA at a final concentration of 10 mmol/L for 20 min. Subsequently, the cells were collected and analysed by flow cytometry after three washes with PBS. Fluorescence microscopy (LX71, Olympus, Tokyo, Japan) was utilized to detect the intracellular ROS at an excitation wavelength of 488 nm and emission wavelength of 525 nm.

Cytotoxicity Assay

HepG2 cells were seeded into 96-well-microplates at a density of 5×10^3 cells per well and incubated overnight. Afterwards, the culture medium was replaced with fresh DMEM containing different concentrations of PI-103, IR820 NBs, or both reagents. The cells incubated with IR820 NBs were treated with and without US irradiation (frequency: 1 MHz, power density: 3 W/cm^2, duty cycle: 50%) for 90 s. After 24 h of incubation, HepG2 cell viability was assessed by the cell counting kit 8 (CCK–8) assay. According to manufacturer's protocol, 10 μL of CCK–8 solution (Beyotime Institute of Biotechnology, Jiangsu, China) was added to each well and the plates were incubated for 60 min at 37 °C in the dark. The absorption of each well was measured using a microplate reader (Promega Corp, Madison, WI, USA) at a wavelength of 450 nm, and the combination index (CI) value of the synergetic treatment was calculated using CompuSyn software.[19]

Cell Apoptosis Assay

Following manufacturer's instructions, cell apoptosis was determined with the PE Annexin V Apoptosis Detection Kit

(BD Biosciences, Franklin Lakes, NJ, USA). After HepG2 cells were collected and washed with cold PBS three times, approximately 1×10^5 cells were resuspended in 500 μL of 1× binding buffer and stained with 5 μL phycoerythrin Annexin V and 5 μL 7-aminoactivatin (7-AAD) for 15 min in the dark. The apoptosis rate of each group was immediately measured by flow cytometry (BD Biosciences, USA). For this purpose, apoptotic cells were stained with PE Annexin V^+/7-AAD^- (early apoptotic cells) and PE Annexin V^+/7-AAD^+ (late apoptotic cells).

Mitochondrial Membrane Potential Assay

For early apoptosis detection, a JC-1 fluorescence probe (Beyotime, Jiangsu, China) was used to analyse the mitochondrial membrane potential (ΔΨm) via fluorescence microscopic imaging. After 24 h of treatment, HepG2 cells were stained with JC-1 at 37 °C for 20 min in the dark and then washed twice with JC-1 staining buffer before detection. The average fluorescence intensity was determined by ImageJ software (National Institutes of Health, Bethesda, MD, USA). A decrease in the fluorescence intensity ratio of the JC-1 aggregate (red) to the monomer (green) indicated the loss of ΔΨm.

Transwell Analysis

Cell migration was assessed using transwell plates (Costar, USA) containing chamber inserts with pore sizes of 8.0 μm. Approximately 1×10^4 cells cultured in 100 μL of the serum-free medium were seeded in the upper chamber, and 800 μL medium containing 10% FBS was added to the lower chamber as an inducing agent. After 24 h of incubation, the cells migrated to the lower membrane surface were fixed with 4% paraformaldehyde solution and stained with 0.5% crystal violet solution for 30 min. After carefully washing with distilled water twice, the cells were quantified by counting three fields.

Statistical Analysis

Statistical analysis was performed using GraphPad Prism 8 software (San Diego, CA, USA). All data were presented as mean ± standard deviation, and the $p < 0.05$ level was considered statistically significant. Student's *t*-test was used to evaluate the statistical difference between two groups, and one-way analysis of variance was conducted to compare multiple groups.

Results

Fabrication and Characterization of IR820 NBs

As observed by TEM, IR820 NBs with a spherical morphology were well dispersed in an aqueous solution, and the particle size did not significantly change after storage at 37 °C for 48 h, which confirmed the stability of IR820 NBs (Figure 1B and C). Their particle size measured by DLS was 545.5±93.1 nm with a mean PDI of 0.255 (Figure 1D), which was in agreement with the TEM results. The mean zeta potential of the NB surface was −5.19±1.73 mV (Figure 1E). To verify the successful formation of IR820 NBs, absorption spectra were recorded for IR820, IR820 NBs, and pure NBs. The characteristic IR820 absorbance peaks were also observed for the IR820 NBs (Figure 1F), indicating the incorporation of IR820 into IR820 NBs.

In vitro US Destructibility of IR820 NBs

The US destructibility experiment was assessed in 3 groups: blank (no sonication), IR820 NBs, and NBs. The corresponding fold line diagram of the concentration of NBs is shown in Figure 2. Without US irradiation, the loss of NBs in blank measurements was considered negligible. Attenuation half-life ($t_{1/2}$) of IR820 NBs and NBs were 52.25 s and 55.59 s, respectively, with no significant difference between them ($p > 0.05$). Therefore, IR820 can be effectively released from IR820 NBs under US irradiation through the UTND mechanism.

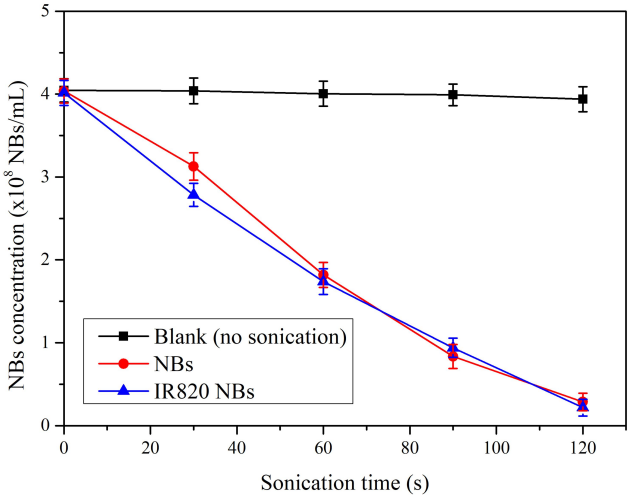

Figure 2 In vitro US destructibility of IR820 NBs.

Intracellular ROS Generation

Intracellular ROS generation in HepG2 cells was examined by a DCFH–DA fluorescent probe. As shown in Figure 3A, very weak fluorescence was detected for the control and IR820 groups, whereas the IR820 + US group exhibited strong green fluorescence, which confirmed the ability of IR820 to serve as a feasible sonosensitizer generating ROS under US irradiation. Noticeably, the fluorescence intensity of IR820 NBs under US irradiation was much higher than that of pure IR820 at the corresponding concentrations, which likely resulted from the amplified cavitation of NBs induced by US irradiation through sonoluminescence.

The quantitative analysis of ROS generation was further performed by flow cytometry (Figure 2B and C). Similarly, the maximal fluorescence intensity was generated by the IR820 NBs + US group, which was almost two times greater than that produced by the IR820 + US group ($p < 0.01$). These results indicate that IR820 NBs can enhance the therapeutic effects of SDT by inducing excessive ROS generation. Thus, IR820 NBs were selected for SDT treatment in the subsequent experiments.

Synergistic Cytotoxicity of PI-103 and SDT to HepG2 Cells

To evaluate the cytotoxicity of PI-103 and SDT, the viability of HepG2 cells was examined by the standard CCK–8 assay after the incubation with PI-103 (concentration: 0–8 μM) or IR820 NBs (concentration: 0–8 μM) for 24 h. As shown in Figure 4A, IR820 NBs demonstrated no obvious cytotoxicity in HepG2 cells even at a high concentration of 8 μM without US irradiation, suggesting the good biocompatibility of IR820 NBs. The treatment with PI-103 or SDT alone reduced the cell viability in a dose-dependent manner, and the half maximal inhibitory concentration (IC_{50}) of PI-103 and SDT to HepG2 cells was 5.021 μM and 3.949 μM, respectively (Figure 4B and C). The survival rate significantly decreased to 25.36±0.34% for the cells treated with 8 μM of IR820 NBs under US

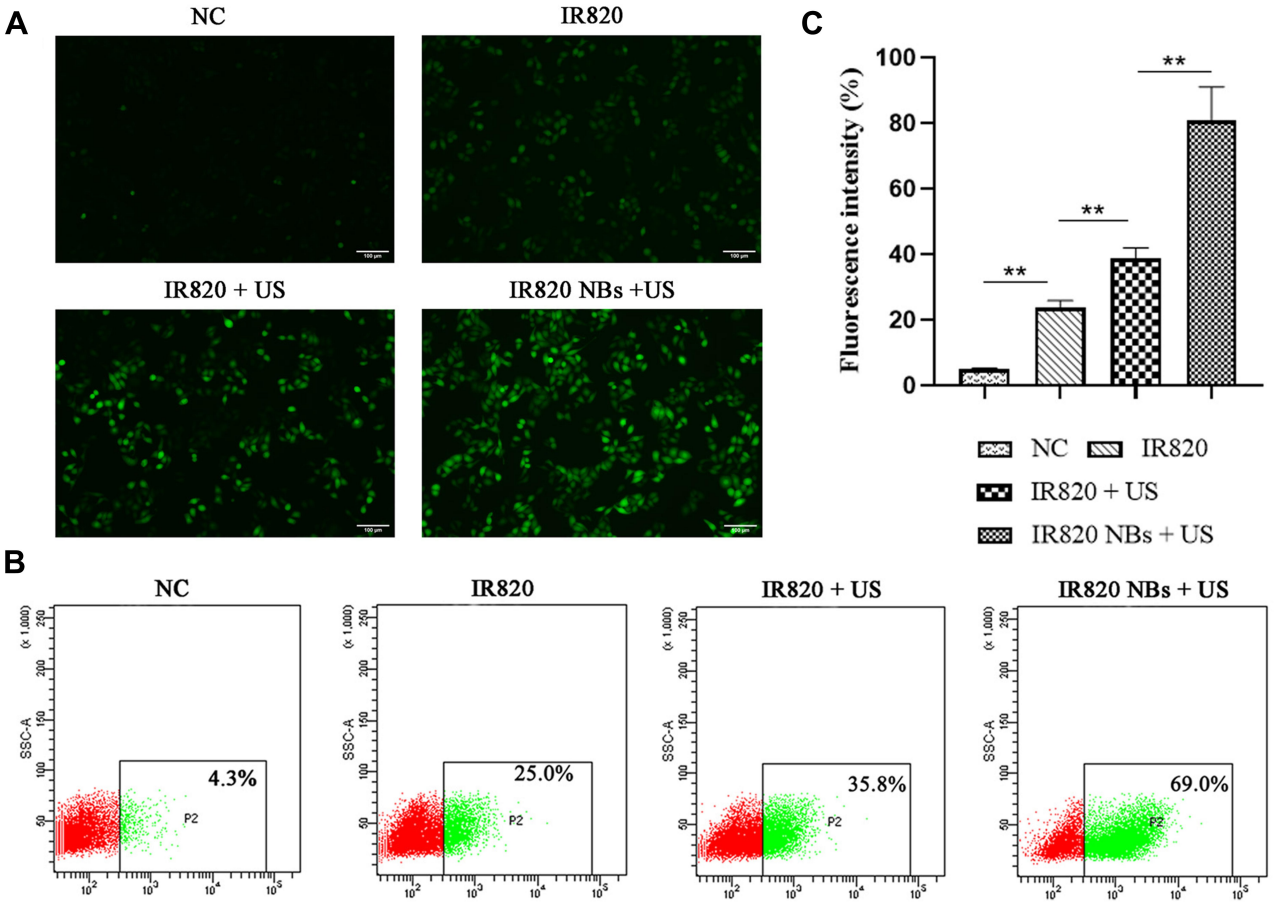

Figure 3 Detection of intracellular ROS generation. (**A**) Fluorescence imaging of HepG2 cells stained by DCFH-DA. (**B**) ROS generation was analyzed by flow cytometry. (**C**) The quantification of fluorescence intensity in different groups. **p<0.01.

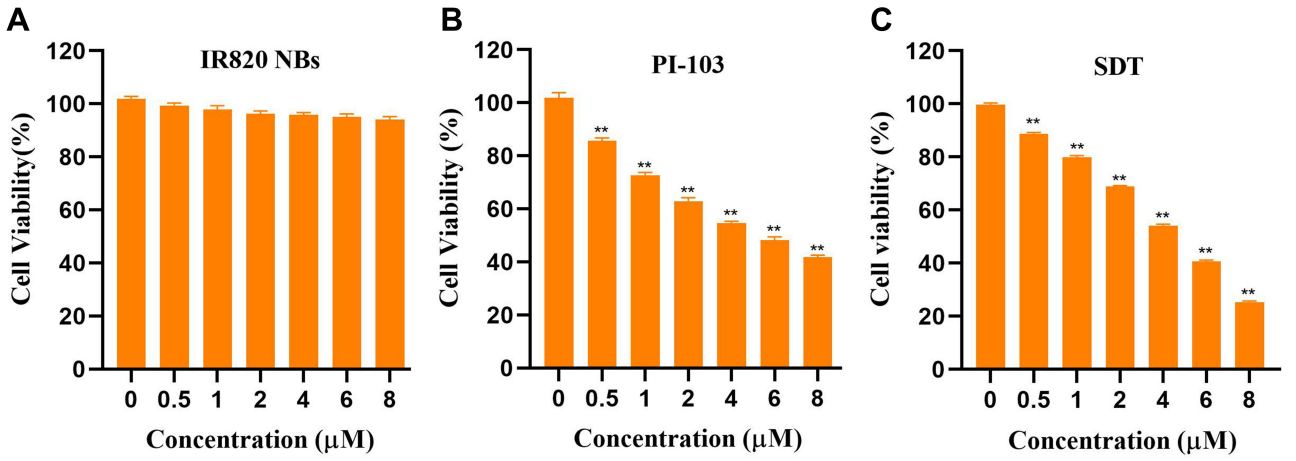

Figure 4 Cytotoxic effect of PI-103 and SDT in HepG2 cells. (**A**) HepG2 cells were treated with IR820 NBs for 24 h without US irradiation, and cell viabilities were analyzed by CCK-8 assay. (**B**) HepG2 cells were treated with PI-103 (concentration: 0–8 μM) for 24 h, and cell viabilities were analyzed by CCK-8 assay. (**C**) HepG2 cells were treated with IR820 NBs (concentration: 0–8 μM; ultrasound: 1 MHz, 3 W/cm2) for 24 h, and cell viabilities were analyzed by CCK-8 assay. **p<0.01.

irradiation (as compared with that of the control group, $p < 0.01$), indicating that IR820 NBs acted as potential nano-sonosensitizers for SDT.

To further investigate the synergistic effects of PI-103 and SDT, HepG2 cells were treated with PI-103 and IR820 NBs at a concentration ratio of 1:1 and subjected to US irradiation for 90 s. The results revealed that PI-103 combined with SDT decreased the cell viability more significantly than with SDT alone. Moreover, the CI value of the combination of 8 μM PI-103 and 8 μM IR820 NBs was equal to 0.18, which indicated the synergistic cytotoxicity of PI-103 and SDT to HepG2 cells (Table 1).

PI-103 Enhancement of SDT-Induced Cell Apoptosis

To determine a possible correlation between the decrease in cell viability and cell apoptosis, HepG2 cells were treated with PI-103, SDT, and their combination for 24 h. Subsequently, cell apoptosis was accessed by flow cytometry after the double staining with Annexin V and 7-AAD. As shown in Figure 5A, the IR820 NB-mediated SDT induced noticeable apoptosis in HepG2 cells. Comparatively, only 5.17±2.00% and 15.87 ±1.95% apoptotic cells were detected in the control group and PI-103 group, respectively. As shown in Figure 5B, the combination of PI-103 and SDT increased the number of apoptotic cells as compared with those in the other groups treated with single agents. After adding PI-103 to SDT, the apoptotic rate increased from 53.50±1.83% to 77.37±1.78% ($p < 0.01$), indicating that PI-103 significantly enhanced the SDT-induced apoptosis in HepG2 cells.

Effect of Mitochondrial Membrane Depolarization on Cell Apoptosis

To evaluate the relationship between the cell apoptosis induced by the combined treatment and the mitochondrial function, ΔΨm changes for the HepG2 cells stained by JC-1 were determined by fluorescence microscopic imaging. As shown in Figure 6A, the treated cells in the control and PI-103 groups exhibited intense red fluorescence, while the SDT-treated cells mainly produced green fluorescence. In addition, the combined treatment

Table 1 Synergistic Cytotoxicity of the Combination Treatment of PI-103 and SDT in HepG2 Cells

PI-103		SDT		PI-103 + SDT	
Dose (μM)	IR (%)	Dose (μM)	IR (%)	IR (%)	CI
0.5	14.3 ± 1.1	0.5	11.2 ± 0.5	31.0 ± 0.2	0.58
1	27.2 ± 1.0	1	20.1 ± 0.6	36.3 ± 0.4	0.87
2	37.1 ± 1.4	2	31.0 ± 0.3	68.1 ± 0.2	0.39
4	45.4 ± 0.7	4	45.9 ± 0.6	84.5 ± 0.5	0.27
6	51.8 ± 1.2	6	59.4 ± 0.6	89.3 ± 0.4	0.26
8	58.1 ± 0.7	8	74.6 ± 0.3	94.2 ± 0.2	0.18

Abbreviations: IR, inhibition rate; CI, combination index.

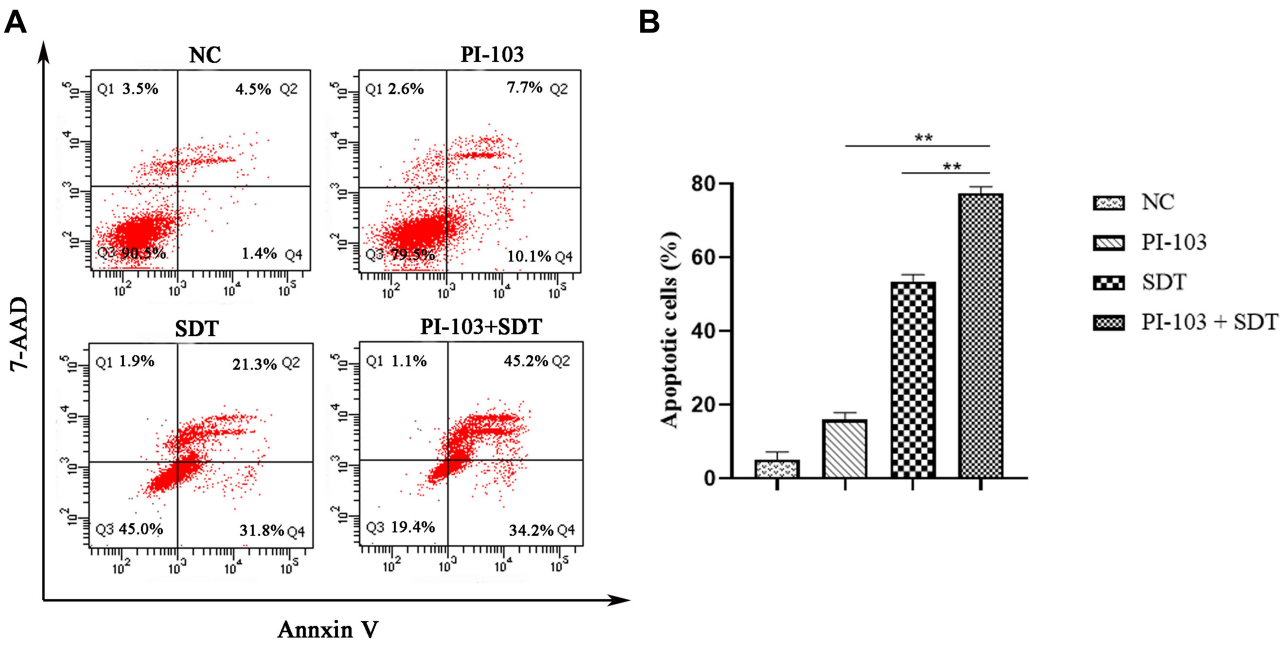

Figure 5 PI-103 enhanced SDT induced cell apoptosis. (**A**) HepG2 cells were treated with PI-103, SDT or both for 24 h, and then stained with Annexin-V and 7-AAD before being analyzed by flow cytometry. (**B**) Statistical results from three independent experiments of cell apoptosis in HepG2 cells. **p<0.01.

further increased the green fluorescence intensity of HepG2 cells, indicating a significant loss of ΔΨm. As mitochondrial depolarization was demonstrated by the decrease in the JC-1 aggregate/monomer ratio,[20] the loss of ΔΨm was quantified by measuring the average fluorescence intensity. After the combined treatment with PI-103 and SDT, the JC-1 aggregate within mitochondria converted to a monomeric form and significantly decreased the aggregate/monomer ratio (Figure 6B). These data illustrated the involvement of mitochondrial membrane depolarization in the cell apoptosis induced by the combined treatment.

Suppression of HepG2 Migration Ability

Cell migration is a fundamental function of tumour cell metastasis.[21] In this study, we evaluated the migration of HepG2 cells by the transwell assay to investigate the inhibitory effect of the combined treatment on HCC metastatic processes. As shown in Figure 7A, the combination of PI-103 and SDT significantly inhibited the migration of HepG2 cells. The average number of migrated cells in the co-treated group was dramatically reduced as compared with those in the single-treated groups ($P < 0.01$, Figure 7B). Hence, the combined treatment suppressed the migration ability of HepG2 cells.

Discussion

Despite the multitude of research studies and clinical trials involving HCC treatment, the disadvantages of the currently used therapies, such as low selectivity and long-term adverse effects, require the development of more effective therapeutic strategies.[22] SDT, a non-invasive US-triggered therapeutic approach, has attracted much attention in the cancer treatment field.[23] A previous study confirmed that SDT alone or in combination with other anticancer agents exhibited a promising anti-HCC performance.[24] However, the low biocompatibility and chemical instability of traditional sonosensitizers limit the therapeutic efficacy of SDT and its possible clinical applications.[25]

Recently, nanoparticles with encapsulated therapeutic compounds have started playing an important role in anticancer research as they can passively accumulate in malignant lesions due to the enhanced permeability and retention effect.[26,27] Among these particles, gas-filled NBs are widely used as delivery vectors for sonosensitizers because of their good biocompatibility.[28,29] The IR820 NBs prepared in this study had spherical shapes with an average particle size of 545.5±93.1 nm (Figure 1D). Previous research also showed that the NBs encapsulated in sonosensitizers could significantly enhance the therapeutic effect of SDT by promoting ROS accumulation.[30] In the present study, excessive ROS

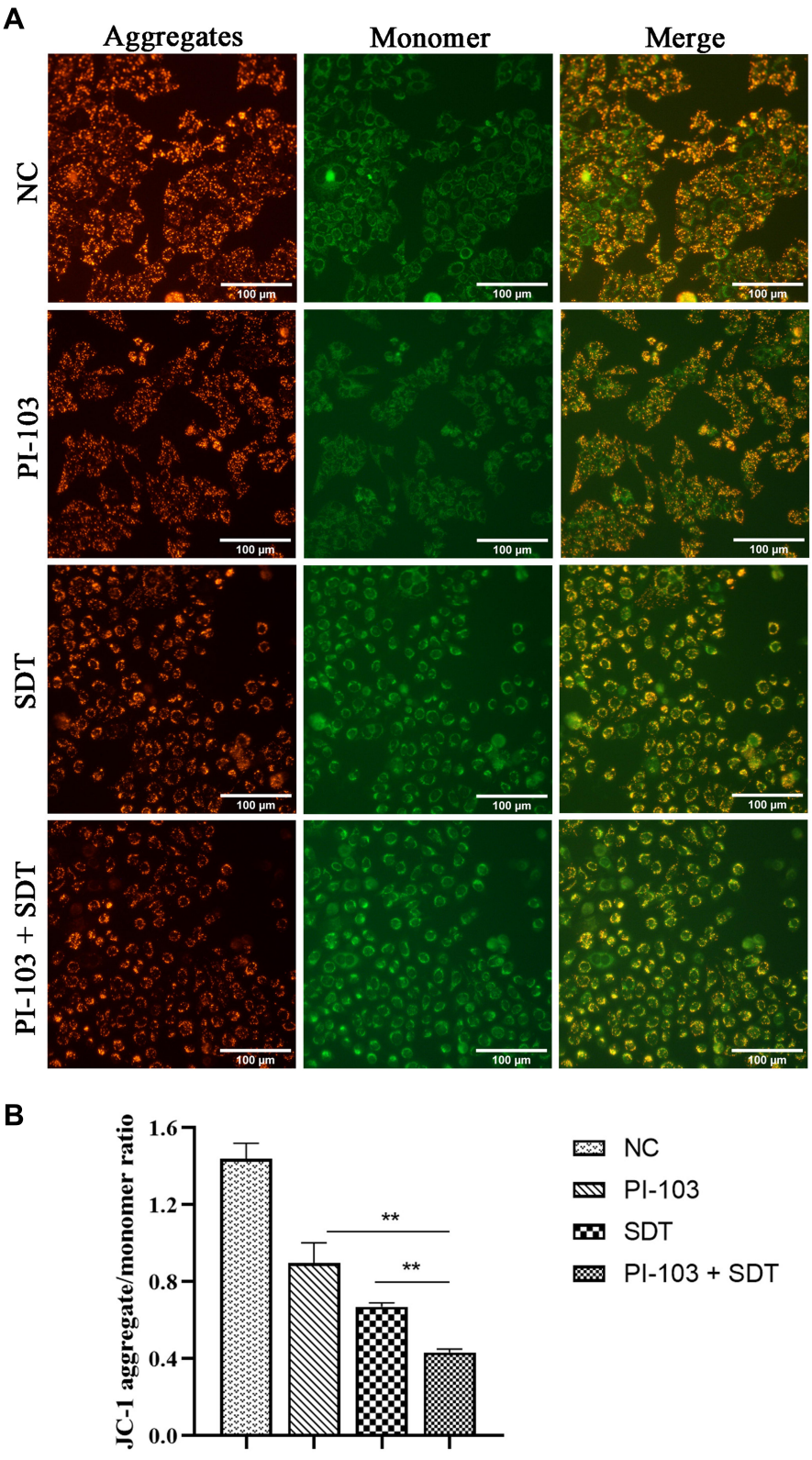

Figure 6 Involvement of mitochondrial membrane depolarization in combination treatment induced apoptosis. (**A**) Fluorescence microscopic imaging of HepG2 cells stained with JC-1 under different treatments. (**B**) The aggregate/monomer fluorescence intensity ratio of JC-1. **p<0.01.

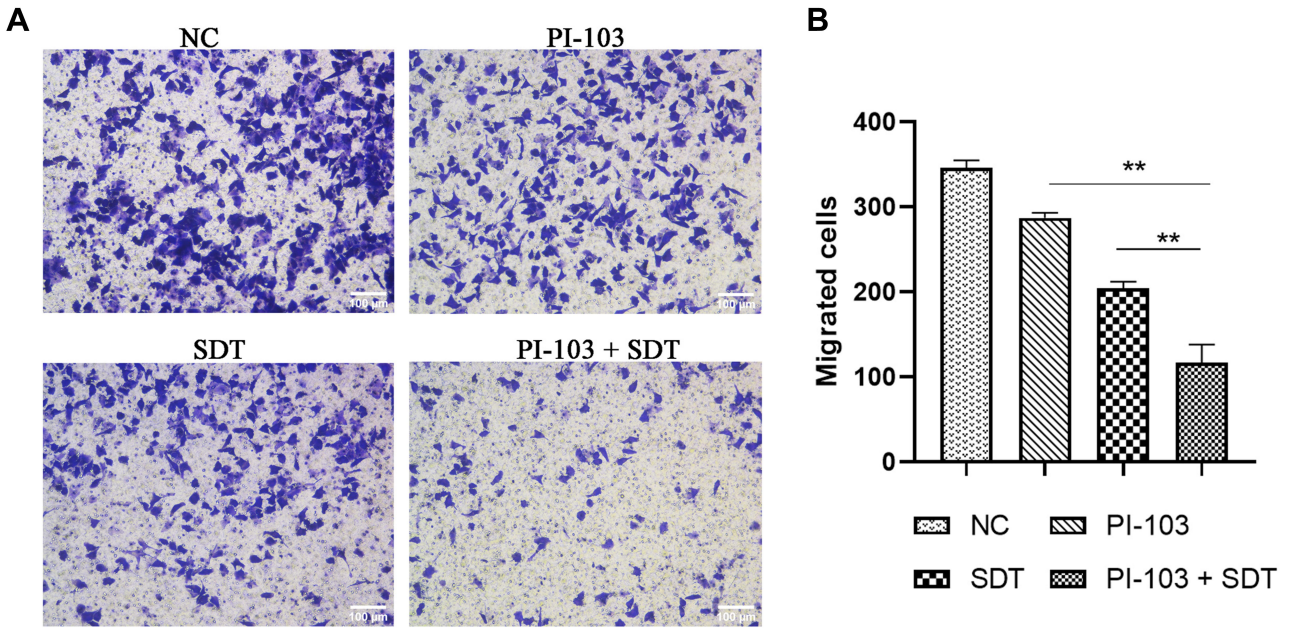

Figure 7 Combination treatment suppressed migration viability of HepG2 cells. (**A**) Transwell assay was performed in HepG2 cells to investigate the inhibitory effect of combination treatment on HCC metastatic processes. (**B**) Quantitation of migrated cell number of HepG2 cells. **p<0.01.

production was detected in the HepG2 cells treated with IR820 NBs under US irradiation (Figure 3). To the best of our knowledge, IR820 has not been previously used as a sonosensitizer for SDT. The results of this study confirmed that IR820 NBs acted as an efficacious nano-sonosensitizer during the SDT treatment of HCC.

ROS generation was found to be the basis of SDT therapeutic effects and played an important role in triggering cell cytotoxicity.[31] Previous studies have shown that ROS accumulation can induce the mechanical disruption of membranes, protein degradation, and DNA fragmentation in cancer cells.[32] The IR820 NBs-mediated SDT in this study reduced the cell viability in a dose-dependent manner (Figure 4C). Furthermore, ROS accumulation produced an inhibitory effect on HCC proliferation via the PI3K/AKT/mTOR signaling pathway, which was mainly activated in advanced HCC due to the poor prognosis of patients.[33,34]

PI-103 is a synthetic small molecule that selectively inhibits class I PI3K and mTOR.[35] It has been used in preclinical studies to demonstrate antiproliferative effects against several cancer types.[36] As PI-103 was found to be potentially usable in combinations with other types of anticancer therapies, it was important to develop inhibitor-based combined strategies with synergistic treatment effects.[37] Thus, we investigated the synergistic effects of SDT and PI-103 for anti-HCC treatment. As proliferation inhibition was examined in vitro, the SDT combined with PI-103 produced stronger inhibitory effects than those of HCC monotherapy, and the corresponding CI value reached 0.18 (Table 1).

A previous study revealed that SDT promoted cell apoptosis through the mitochondria-caspase signalling pathway and induced the expression of the proapoptotic effector Bax.[38] In addition, PI-103 was reported to accelerate cell apoptosis by promoting Annexin V binding and nuclear fragmentation.[39] To identify the mechanisms of the synergistic inhibition induced by the combined treatment, cell apoptosis was examined by the flow cytometric analysis using the PE Annexin V Apoptosis assay. Consistent with the previous data, a larger degree of apoptosis was obtained for the co-treated HepG2 cells, as evidenced by the increase in the apoptosis rate from 53.50±1.83% to 77.37±1.78% (Figure 5B).

Mitochondria integrated various decisive events of the intrinsic apoptotic pathway, and mitochondrial membrane depolarization resulting in the loss of ΔΨm confirmed the apoptosis in HepG2 cells.[40] As the ROS-induced oxidative injury destroys the stability of the mitochondrial membrane, cytochrome C is released from mitochondria and conjugates the apoptotic protein activator in the cytoplasm, leading to the cell apoptosis by proteolysis.[41] We also investigated the effects of SDT and PI-103 on the damage caused to ΔΨm using the JC-1 method. The combined

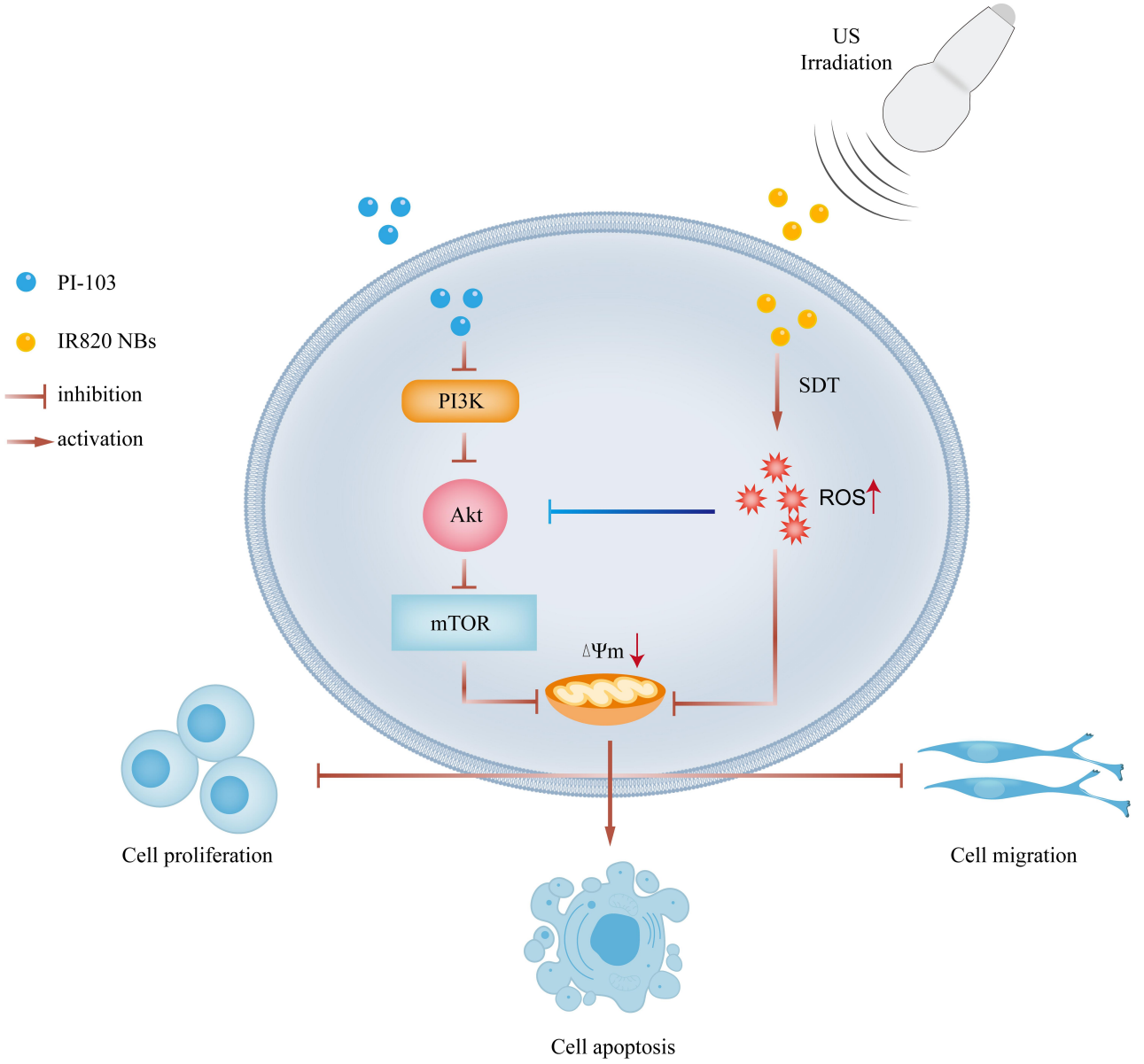

Figure 8 Overview of combination treatment of sonodynamic therapy and PI-103 in HCC cells.

treatment significantly reduced the JC-1 aggregate-to-monomer fluorescence intensity ratio, indicating the loss of ΔΨm and mitochondrial dysfunction (Figure 6B). These results suggest that the combination of SDT and PI-103 played a potentially important role in regulating the mitochondrial function and inducing apoptosis in HepG2 cells, which helped to elucidate the HCC synergistic inhibition mechanism.

Because the proliferation and migration of cancer cells are strongly related to the oxidative stress and mitochondrial function,[42] the migration of HepG2 cells was examined by the transwell assay to investigate the role of the combined therapy in regulating HCC metastatic processes. As a minimal number of HepG2 cells migrated through the lower chamber after the combined treatment, the latter significantly inhibited the HepG2 cell migration (Figure 7).

The methodology used in the present study also has some limitations. First, although the obtained experimental results confirmed the synergistic effects of SDT and PI-103 on the anti-HCC treatment efficiency, the underlying reaction mechanisms have not been fully clarified. Second, the combined strategy was applied only to the HepG2 cell line, while its effects on other HCC cell lines have not

been examined. Future research studies will involve an in vivo xenograft model to verify the safety of the proposed method and validate the in vitro results.

Conclusion

The data obtained in the present study not only confirmed the possibility of using IR820 NBs as a novel sonosensitizer for SDT, but also suggested new HCC treatment strategies. We demonstrated for the first time that SDT combined with PI-103 exhibited synergistic inhibitory effects on HCC by restricting cell proliferation and migration and promoting cell apoptosis through the mitochondrial pathway (Figure 8). Our findings may help to develop new non-invasive cancer treatment approaches with good clinical application prospects.

Acknowledgments

The human HCC cell line HepG2 was obtained from the Institute of Cancer Research affiliated with the Harbin Medical University and approved by Ethics Committee of Harbin Medical University.

Author Contributions

Methodology, H.Y.; validation, H.Y., H.T.; data curation, X.H.; writing—original draft preparation, H.Y.; writing—review and editing, W.C.; supervision, H.J.; project administration, W.C.; funding acquisition, W.C and H.J. All authors contributed to data analysis, drafting or revising the article, have agreed on the journal to which the article will be submitted, gave final approval of the version to be published, and agree to be accountable for all aspects of the work.

Funding

This research was supported by the National Natural Science Foundation of China (grant 81873900 to W.C.; grant 81801709 to H.J.).

Disclosure

The authors report no conflicts of interest in this work.

References

1. Villanueva A, Longo DL. Hepatocellular carcinoma. *N Engl J Med*. 2019;380(15):1450–1462. doi:10.1056/NEJMra1713263
2. Ma S, Sun J, Guo Y, et al. Combination of AAV-TRAIL with miR-221-zip therapeutic strategy overcomes the resistance to TRAIL induced apoptosis in liver cancer. *Theranostics*. 2017;7(13):3228–3242. doi:10.7150/thno.19893
3. Yumita N, Nishigaki R, Umemura K, Umemura S. Hematoporphyrin as a sensitizer of cell-damaging effect of ultrasound. *Jpn J Cancer Res*. 1989;80(3):219–222. doi:10.1111/j.1349-7006.1989.tb02295.x
4. Pan X, Bai L, Wang H, et al. Metal-organic-framework-derived carbon nanostructure augmented sonodynamic cancer therapy. *Adv Mater*. 2018;30(23):e1800180. doi:10.1002/adma.201800180
5. Zhu P, Chen Y, Shi J. Nanoenzyme-augmented cancer sonodynamic therapy by catalytic tumor oxygenation. *ACS Nano*. 2018;12(4):3780–3795. doi:10.1021/acsnano.8b00999
6. Lin X, Song J, Chen X, Yang H. Ultrasound-activated sensitizers and applications. *Angew Chem Int Ed Engl*. 2019.
7. Li X, Zhao X, Pardhi D, et al. Folic acid modified cell membrane capsules encapsulating doxorubicin and indocyanine green for highly effective combinational therapy in vivo. *Acta Biomater*. 2018;74:374–384. doi:10.1016/j.actbio.2018.05.006
8. Hou X, Zhou H, Wang L, et al. Multifunctional near-infrared dye-magnetic nanoparticles for bioimaging and cancer therapy. *Cancer Lett*. 2017;390:168–175. doi:10.1016/j.canlet.2016.12.026
9. Chen Q, Liang C, Wang C, Liu Z. An imagable and photothermal "abraxane-like" nanodrug for combination cancer therapy to treat subcutaneous and metastatic breast tumors. *Adv Mater*. 2015;27(5):903–910. doi:10.1002/adma.201404308
10. Liao J, Wei X, Ran B, Peng J, Qu Y, Qian Z. Polymer hybrid magnetic nanocapsules encapsulating IR820 and PTX for external magnetic field-guided tumor targeting and multifunctional theranostics. *Nanoscale*. 2017;9(7):2479–2491. doi:10.1039/C7NR00033B
11. De Cock I, Zagato E, Braeckmans K, et al. Ultrasound and microbubble mediated drug delivery: acoustic pressure as determinant for uptake via membrane pores or endocytosis. *J Control Release*. 2015;197:20–28. doi:10.1016/j.jconrel.2014.10.031
12. Kim J, Jo C, Lim WG, et al. Programmed nanoparticle-loaded nanoparticles for deep-penetrating 3d cancer therapy. *Adv Mater*. 2018;e1707557.
13. Liu Y, Zhang D, Qiao ZY, et al. A peptide-network weaved nanoplatform with tumor microenvironment responsiveness and deep tissue penetration capability for cancer therapy. *Adv Mater*. 2015;27(34):5034–5042. doi:10.1002/adma.201501502
14. Dong C, Jiang Q, Qian X, et al. A self-assembled carrier-free nanosonosensitizer for photoacoustic imaging-guided synergistic chemo-sonodynamic cancer therapy. *Nanoscale*. 2020;12(9):5587–5600. doi:10.1039/C9NR10735E
15. Rebouissou S, Nault JC. Advances in molecular classification and precision oncology in hepatocellular carcinoma. *J Hepatol*. 2020;72(2):215–229. doi:10.1016/j.jhep.2019.08.017
16. Tan JL, Li F, Yeo JZ, et al. New high-throughput screening identifies compounds that reduce viability specifically in liver cancer cells that express high levels of SALL4 by inhibiting oxidative phosphorylation. *Gastroenterology*. 2019;157(6):1615–1629.e17. doi:10.1053/j.gastro.2019.08.022
17. Yao W, Lin Z, Shi P, et al. Delicaflavone induces ROS-mediated apoptosis and inhibits PI3K/AKT/mTOR and Ras/MEK/Erk signaling pathways in colorectal cancer cells. *Biochem Pharmacol*. 2020;171:113680. doi:10.1016/j.bcp.2019.113680
18. Tinkov S, Winter G, Coester C, Bekeredjian R. New doxorubicin-loaded phospholipid microbubbles for targeted tumor therapy: part I–formulation development and in-vitro characterization. *J Control Release*. 2010;143(1):143–150. doi:10.1016/j.jconrel.2009.12.026
19. Chou TC, Motzer RJ, Tong Y, Bosl GJ. Computerized quantitation of synergism and antagonism of taxol, topotecan, and cisplatin against human teratocarcinoma cell growth: a rational approach to clinical protocol design. *J Natl Cancer Inst*. 1994;86(20):1517–1524. doi:10.1093/jnci/86.20.1517
20. Smiley ST, Reers M, Mottola-Hartshorn C, et al. Intracellular heterogeneity in mitochondrial membrane potentials revealed by a J-aggregate-forming lipophilic cation JC-1. *Proc Natl Acad Sci U S A*. 1991;88(9):3671–3675. doi:10.1073/pnas.88.9.3671

21. Su Z, Yang Z, Xu Y, Chen Y, Yu Q. Apoptosis, autophagy, necroptosis, and cancer metastasis. *Mol Cancer*. 2015;14(1):48. doi:10.1186/s12943-015-0321-5
22. Yu L, Xu F, Gao L. Predict new therapeutic drugs for hepatocellular carcinoma based on gene mutation and expression. *Front Bioeng Biotechnol*. 2020;8:8. doi:10.3389/fbioe.2020.00008
23. Li G, Wang S, Deng D, et al. Fluorinated chitosan to enhance transmucosal delivery of sonosensitizer-conjugated catalase for sonodynamic bladder cancer treatment post-intravesical instillation. *ACS Nano*. 2020;14(2):1586–1599. doi:10.1021/acsnano.9b06689
24. Zhuang D, Han J, Bi L, et al. Sonodynamic effect of hematoporphyrin monomethyl ether on ligature-induced periodontitis in rats. *Drug Des Devel Ther*. 2015;9:2545–2551. doi:10.2147/DDDT.S82347
25. Son S, Kim JH, Wang X, et al. Multifunctional sonosensitizers in sonodynamic cancer therapy. *Chem Soc Rev*. 2020;49(11):3244–3261. doi:10.1039/C9CS00648F
26. Gan H, Chen L, Sui X, et al. Enhanced delivery of sorafenib with anti-GPC3 antibody-conjugated TPGS-b-PCL/pluronic P123 polymeric nanoparticles for targeted therapy of hepatocellular carcinoma. *Mater Sci Eng C Mater Biol Appl*. 2018;91:395–403. doi:10.1016/j.msec.2018.05.011
27. Tang X, Lyu Y, Xie D, Li A, Liang Y, Zheng D. Therapeutic effect of sorafenib-loaded TPGS-b-PCL nanoparticles on liver cancer. *J Biomed Nanotechnol*. 2018;14(2):396–403. doi:10.1166/jbn.2018.2529
28. Zhang Y, Xie C, Li A, et al. PKI-587 enhances chemosensitivity of oxaliplatin in hepatocellular carcinoma through suppressing DNA damage repair pathway (NHEJ and HR) and PI3K/AKT/mTOR pathway. *Am J Transl Res*. 2019;11(8):5134–5149.
29. Tang X, Chen L, Li A, et al. Anti-GPC3 antibody-modified sorafenib-loaded nanoparticles significantly inhibited HepG2 hepatocellular carcinoma. *Drug Deliv*. 2018;25(1):1484–1494. doi:10.1080/10717544.2018.1477859
30. Ma A, Chen H, Cui Y, et al. Metalloporphyrin complex-based nanosonosensitizers for deep-tissue tumor theranostics by noninvasive sonodynamic therapy. *Small*. 2019;15(5):e1804028. doi:10.1002/smll.201804028
31. Chen J, Ding J, Wang Y. Sequentially responsive shell-stacked nanoparticles for deep penetration into solid tumors. *Adv Mater*. 2017;29(32):1701170. doi:10.1002/adma.201701170
32. Shi J, Chen Z, Wang B, Wang L, Lu T, Zhang Z. Reactive oxygen species-manipulated drug release from a smart envelope-type mesoporous titanium nanovehicle for tumor sonodynamic-chemotherapy. *ACS Appl Mater Interfaces*. 2015;7(51):28554–28565. doi:10.1021/acsami.5b09937
33. Tang X, Li A, Xie C, et al. The PI3K/mTOR dual inhibitor BEZ235 nanoparticles improve radiosensitization of hepatoma cells through apoptosis and regulation DNA repair pathway. *Nanoscale Res Lett*. 2020;15(1):63. doi:10.1186/s11671-020-3289-z
34. Jiang S, Wang Q, Feng M, et al. C2-ceramide enhances sorafenib-induced caspase-dependent apoptosis via PI3K/AKT/mTOR and Erk signaling pathways in HCC cells. *Appl Microbiol Biotechnol*. 2017;101(4):1535–1546. doi:10.1007/s00253-016-7930-9
35. Raynaud FI, Eccles S, Clarke PA, et al. Pharmacologic characterization of a potent inhibitor of class I phosphatidylinositide 3-kinases. *Cancer Res*. 2007;67(12):5840–5850. doi:10.1158/0008-5472.CAN-06-4615
36. Knight ZA, Gonzalez B, Feldman ME, et al. A pharmacological map of the PI3-K family defines a role for p110alpha in insulin signaling. *Cell*. 2006;125(4):733–747. doi:10.1016/j.cell.2006.03.035
37. Wu B, Li A, Zhang Y, et al. Resistance of hepatocellular carcinoma to sorafenib can be overcome with co-delivery of PI3K/mTOR inhibitor BEZ235 and sorafenib in nanoparticles. *Expert Opin Drug Deliv*. 2020;17(4):573–587. doi:10.1080/17425247.2020.1730809
38. Pan X, Wang H, Wang S, et al. Sonodynamic therapy (SDT): a novel strategy for cancer nanotheranostics. *Sci China Life Sci*. 2018;61(4):415–426. doi:10.1007/s11427-017-9262-x
39. Maurya AK, Vinayak M. PI-103 attenuates PI3K-AKT signaling and induces apoptosis in murineT-cell lymphoma. *Leuk Lymphoma*. 2017;58(5):1153–1161. doi:10.1080/10428194.2016.1225207
40. Kroemer G, Galluzzi L, Brenner C. Mitochondrial membrane permeabilization in cell death. *Physiol Rev*. 2007;87(1):99–163.
41. Li W, Liu Y, Wang B, et al. Protective effect of berberine against oxidative stress-induced apoptosis in rat bone marrow-derived mesenchymal stem cells. *Exp Ther Med*. 2016;12(6):4041–4048. doi:10.3892/etm.2016.3866
42. Zhang X, Gibhardt CS, Will T, et al. Redox signals at the ER-mitochondria interface control melanoma progression. *EMBO J*. 2019;38(15):e100871. doi:10.15252/embj.2018100871